AFGL-TR-88-0056

SSS-IR-88-9311
W/O 11304

POLAR 2.0 Validation and Preflight SPEAR I Calculations

G. A. Jongeward
M. J. Mandell
J. Lilley
I. Katz

S-CUBED
A Division of Maxwell Laboratories, Inc.
P. O. Box 1620
La Jolla, CA 92038

February 1988

Scientific Report No. 7

AIR FORCE GEOPHYSICS LABORATORY
AIR FORCE SYSTEMS COMMAND
UNITED STATES AIR FORCE
HANSCOM AIR FORCE BASE
MASSACHUSETTS 01731

UNCLASSIFIED
SECURITY CLASSIFICATION OF THIS PAGE

REPORT DOCUMENTATION PAGE

1a REPORT SECURITY CLASSIFICATION Unclassified	1b RESTRICTIVE MARKINGS
2a SECURITY CLASSIFICATION AUTHORITY N/A	3 DISTRIBUTION / AVAILABILITY OF REPORT Approved for public release; distribution unlimited
2b DECLASSIFICATION / DOWNGRADING SCHEDULE N/A	
4 PERFORMING ORGANIZATION REPORT NUMBER(S) SSS-R-88-9311	5 MONITORING ORGANIZATION REPORT NUMBER(S) AFGL-TR-88-0056
6a NAME OF PERFORMING ORGANIZATION S-CUBED, A Division of Maxwell Laboratories, Inc. 6b OFFICE SYMBOL (If applicable)	7a NAME OF MONITORING ORGANIZATION Air Force Geophysics Laboratory
6c ADDRESS (City, State, and ZIP Code) P. O. Box 1620 La Jolla, CA 92038-1620	7b ADDRESS (City, State, and ZIP Code) Hanscom Air Force Base MA 01731
8a NAME OF FUNDING / SPONSORING ORGANIZATION Air Force Geophysics Laboratory 8b OFFICE SYMBOL (If applicable)	9 PROCUREMENT INSTRUMENT IDENTIFICATION NUMBER F19268-86-C-0056
8c ADDRESS (City, State, and ZIP Code) Hanscom Air Force Base MA 01731	10 SOURCE OF FUNDING NUMBERS PROGRAM ELEMENT NO: 62101F; PROJECT NO: 7601; TASK NO: 30; WORK UNIT ACCESSION NO: AA

11 TITLE (Include Security Classification)

Polar 2.0 Validation and Preflight SPEAR I Calculations

12 PERSONAL AUTHOR(S)
G. A. Jongeward, M. J. Mandell, J. R. Lilley, I. Katz

13a TYPE OF REPORT	13b TIME COVERED	14 DATE OF REPORT (Year, Month, Day)	15 PAGE COUNT
Interim technical report no. 7	FROM 1/88 TO 2/88	February, 1988	32

16 SUPPLEMENTARY NOTATION

17 COSATI CODES		
FIELD	GROUP	SUB-GROUP

18 SUBJECT TERMS (Continue on reverse if necessary and identify by block number)
Magnetosheath, magnetic limiting, space charge, SPEAR I, current collection

19 ABSTRACT (Continue on reverse if necessary and identify by block number)

We present a description of the POLAR 2.0 code and data structure. POLAR 2.0 calculations of the self-consistent magnetosheath of a sphere in a magnetic field are presented and shown to be consistent with the Parker-Murphy limits. The POLAR code is shown to agree with the results of a 2-dimensional code for this symmetric case. Preflight SPEAR II calculation of the current distribution to the spheres, booms, and rocket body were performed for two of the voltage configurations. These results are presented here and compared with corresponding nonself-consistent calculations using the NASCAP/LEO code.

20 DISTRIBUTION / AVAILABILITY OF ABSTRACT ☐ UNCLASSIFIED/UNLIMITED ☐ SAME AS RPT. ☐ DTIC USERS	21 ABSTRACT SECURITY CLASSIFICATION Unclassified
22a NAME OF RESPONSIBLE INDIVIDUAL Dr. David L. Cooke	22b TELEPHONE (Include Area Code) 22c OFFICE SYMBOL AFGL/PHK

DD FORM 1473, 84 MAR 83 APR edition may be used until exhausted. All other editions are obsolete.

SECURITY CLASSIFICATION OF THIS PAGE
UNCLASSIFIED

TABLE OF CONTENTS

POLAR 2.0 VALIDATION AND PREFLIGHT SPEAR I CALCULATIONS

G. A. Jongeward, M. J. Mandell, J. Lilley, and I. Katz
S-CUBED Division of Maxwell Laboratories, Inc.

1. INTRODUCTION

In this report, we present a series of calculations used to test and validate the POLAR 2.0 code. The goal in this first limited validation phase of POLAR 2.0 is to model the electron collection experiment, SPEAR I (Space Power Experiments Aboard Rockets). The POLAR code (hereinafter referred to as POLAR 1.1) was developed by S-CUBED for the Air Force Geophysics Laboratory. It is currently in the second year of a 3-year validation phase. Concurrent with this validation effort, the POLAR 2.0 code is being developed. POLAR 2.0 contains the same physical models as POLAR 1.1 but allows multiple grids. This increased versatility is required when both a large computational grid and localized high resolution are needed. Examples of these situations are: SPEAR I, which has important physical details on the centimeter length scale and produces plasma disturbances meters from the rocket; and the charging of an astronaut in the wake of a polar orbiting shuttle in which the details of the astronaut's suit, extra-vehicular maneuvering unit, and the high voltage shuttle charging must all be resolved.

The report is organized as follows: Section 2. contains an overview of POLAR 2.0 and a brief description of the data structure with a comparison to POLAR 1.1. In Section 3., we give a review of the physical models in POLAR 2.0 that are relevant to the calculations presented here. Section 4. contains test calculations for a 10-cm sphere in a magnetic field. Space charge effects on potentials, magnetic field effects on particle trajectories, and self-consistent magnetosheath calculations are presented. Section 5. contains a description of the SPEAR I object, calculational grid structure, and the results of two preflight calculations of current collection by the SPEAR I experiment. Section 6. compares POLAR 2.0 and NASCAP/LEO calculations of the SPEAR I current collection.

2. OVERVIEW OF POLAR 2.0

2.1 Introduction

The original POLAR code, POLAR 1.1, has been extended to include nested grids. Nested grids allow calculations at higher surface potentials without loss of object surface resolution. Additionally, calculation size limitations have been removed. The approach taken was to modify the computational algorithms of POLAR 1.1 as little as possible by adding multiple grid capabilities at the data handling level. Changes were made in the general data handling routines, the file handlers, and in the calculation modules to deal with grid interfaces.

2.2 General

General data handling has been modified in two areas: the method of storing data on the MSIO files, and the use of the PUFF array. The new MSIO routines can be used by POLAR 1.1. POLAR 2.0 uses multiple-indexed MSIO files. When OPENMS is called to read the file index, the number of keys to be used to address the file records is defined. File 19, the data file containing quantities referred to by name, SRFV and so on, adds a second key for the grid number.

The MRBUF routine, which in POLAR 1.1 sets up the VPROPS common block, has been moved to the PATCHV module. The location of POLAR data in both the MSIO data files and the PUFF array is determined during object definition. This has removed many of the limits on the grid size. The discussion of the PATCHV module describes these modifications in more detail.

The complexity of the data structure used in POLAR 2.0 precludes the use of statement functions to calculate data locations. The statement functions, IPUFAD and IPUFZS, have been replaced by integer functions of the same names. Two new data vectors, SGRD and NSGD, have been added to describe the elements and nodes, respectively, of each grid.

2.3 Object Definition

The main difference between the two versions of POLAR is apparent to the user during object definition. Because POLAR 2.0 is oriented towards multiple grid objects, the definition of the grids and the objects within them is much more

complicated than in POLAR 1.1. The grid structure presently in POLAR 2.0 presumes the eventual addition of generalized geometries to POLAR. Grids may be empty or contain ORIENTed VEHICL denifitions. The outermost grid is used to define the mesh size in meters for all of the inner grids and is also the only one that may be stepped as the POLAR 1.1 calculational grid.

Grids are subject to the following restrictions:

1. Grids must be defined in order of nesting, outer first.
2. Grids must be completely enclosed by any outer grids, although boundaries may be shared.
3. The grid origin must lie on a node in the outer grid.
4. The ratio of the inner to outer mesh size must be an integer greater than *zero*.
5. Grid boundaries must be on nodal planes in the outer grid in order to interpolate boundaries values. This means the grid length must be evenly divisible by the mesh ratio of the grid to the outer grid.
6. Inner grids may not touch other, equal level inner grids. (Not checked for.)

Current restrictions to prevent surface subdivision are as follows:

1. Grid boundaries cannot touch nonzero element table entries in the outer grids.
2. A grid cannot contain objects defined in an outer grid.

In order to help the user maneuver objects into their desired locations in the mesh, several enhancements have been made to ORIENT. Grids may be expanded and/or shifted.

A new module was necessary for mesh and object definition for POLAR 2.0 calculations. This module, PATCHV, combines any number of object definitions created by the POLAR 1.1 modules, VEHICL and ORIENT, with empty grids to produce the final calculation mesh. Presently, PATCHV is an interactive module that builds the mesh from the outer grid into the inner grids. Since all of the grid information, such as nx, ny, and nz, and the number of surfaces are known during mesh definition, the MSIO Files 11, 9, and 19 are dynamically defined. This means, for example, that the POT z slices will probably be found at different index key

locations for different mesh definitions. A permanent stack structure is defined, which contains mesh and vector property information. The locations of pointers and vector definition will also vary from run to run.

Fig. 2.1 shows the pointer and data structure for POLAR 2.0. The figure shows the information as it is placed in the common block CBUF. The information in CBUF breaks into four groups. These are: 1. the pregrid information; 2. the pointers to the grid properties; 3. the vector properties; 4. the data.

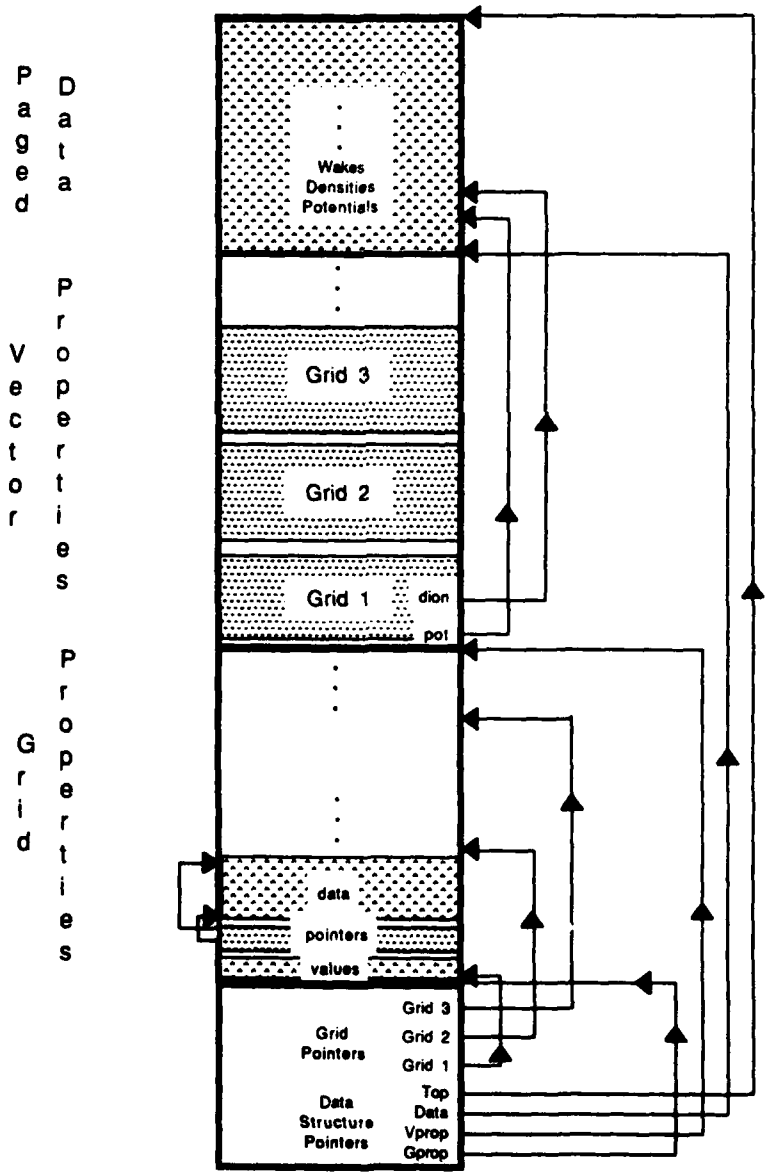

Fig. 2.1

The first group is the pregrid information. This region contains global information such as number of grids and mesh size. It also contains pointers to the start of information on the grids in Region 2 as shown in Fig. 2.1. As indicated, Region 2 starts at location igrid0+1 and contains both values and pointers to the grid properties. The information is grouped by grid, and the grid data follows immediately each grid's pointer information. Region 3 contains the vector property information. The starting point for this information is iavec0+1. The vector properties are stored by grid, so the total length of this region is (number of grids) x (number of vectors) x (number of vector properties). This region contains the IAVEC data of POLAR 1.1. The majority of the information on the vectors is actual values. A few pointers are mixed in with this information: for example, the starting location of the vector data in PUFF is recorded in the second vector property. The final region is for the paged information. This is where all the information read and written to disk by POLAR's data base manager is kept in memory.

2.4 Calculations

The POLAR 1.1 NTERAK module has been divided into two separate executables in POLAR 2.0 for development purposes: POT performs the PWASON and charge calculations, while DENS calculates initial geometric ion densities and the "DIONS" found by "CURREN".

At the present level of development, POLAR 2.0 is not really a very user-friendly code. It has been tested with respect to the algorithms used to handle data sharing between grid boundaries, loops over the grids, and general soundness of the data handling. Work needs to be done to speed up calculations. Several physical features found in POLAR 1.1 have not been fully implemented yet.

3. POLAR 2.0 ELECTRON MAGNETOSHEATH

In this section, we review the physical models and calculational methods that go into a self-consistent calculation of a magnetosheath. We will first discuss a semianalytic approach to calculate the potentials that is valid for symmetric objects. This will be followed by a description of the electron particle-pushing algorithms and finally the computation of a self-consistent magnetosheath.

3.1 Symmetric Potentials

The potential solver in POLAR 2.0 solves Poisson's equation,

$$\nabla^2\phi = -\frac{\rho}{\epsilon_o}$$

The charge density can result from a geometrical ion calculation, barometric law, analytical formulae, or from trajectory tracking. For high voltage electron attracting sheaths, wakes do not produce a significant change in the sheath. As a starting point for a calculation, POLAR 2.0 uses an analytic formula relating the charge density to the potential, $\rho = \rho(\phi,E)$. This analytic relationship produces the correct sheath size and shape for symmetric geometries (spherical, cylindrical, planar) and gives a reasonable starting point for more complex shapes.

The analytical form for $\rho(\phi,E)$ was determined by assuming a form for the convergence factor, $\frac{R_{sheath}}{r}$, namely,

$$\left[\frac{R_{sheath}}{r}\right]^2 = \text{const } E^b\phi^c$$

and then choosing b and c to best approximate the exact relationship in a least squares sense. The following form was found to be an excellent fit over a wide range of temperatures, densities, and potentials:

$$\rho(\phi,E) = \rho_o 2.29\left[\frac{E\lambda_D}{\theta}\right]^{1.262}\left[\frac{\phi}{\theta}\right]^{-.509}\left[\frac{\theta}{4\pi\phi}\right]^{.5}$$

3.2 Electron Particle Pushing

The Earth's magnetic field strongly influences the motion of electrons. A thermal electron has a gyroradius of 2.5 cm. This is much smaller than typical object and sheath dimensions, and much smaller than the 10-m SPEAR I rocket and sheath. Hence, electrons in regions of weak electric field will **ExB** drift and in regions of strong fields will execute complex trajectories, bouncing many times within the sheath. Some electrons will enter noncollecting "trapped" orbits, some will eventually be collected, and still others will leave the sheath. For these reasons, POLAR 1.1 and POLAR 2.0 push electrons differently than ions. In some instances, step pushing is

used; while in other instances, a guiding center, "drift" approximation is used. Electrons, like ions, are pushed using a super particle that has a current, $I = A_{sheath} J_{thermal}$. For each cell, the contribution to the plasma density by a superparticle is $\delta Q = I\tau$, where τ is the time for the particle to cross the cell. First, we discuss the standard step pushing method, followed by a discussion of the drift method.

The equation of motion of an electron in an electric field is

$$m \frac{d\vec{V}}{dt} = e\nabla\phi - e\vec{V}x\vec{B}$$

In zones where the cyclic motion of the electron is comparable to a zone size, step pushing is used. A time step that will produce 10 steps to cross a zone is estimated. The velocity and position are updated using

$$\vec{V}^{i+1} = \vec{V}^{i} + q\vec{E}^{i}\delta t$$

$$\vec{X}^{i+1} = \vec{X}^{i} + \vec{V}^{i}\delta t$$

The rotation of velocity by the magnetic field is computed to second order in δt as,

$$\vec{V}' = \vec{V} + \frac{e}{m}\vec{V}x\vec{B}\delta t + \left[\frac{e}{m}\right]^2 (\vec{V}x\vec{B})x\vec{B}\,\frac{\delta t^2}{2}$$

Using this algorithm for the magnetic field, rotation-produced electron gyroradii accurate to within a percent. This 2-step approximation is much quicker than the more accurate matrix multiple due to the time required to construct and rotate the matrix.

Resolving the drifting motion of electrons in the weak electric field regions is very CPU intensive. To speed the numerics, POLAR uses a drift approximation that breaks the motion into two components. The velocity and acceleration parallel to **B** is unchanged; while perpendicular to **B**, the velocity is the drift velocity with no acceleration. Specifically, for the parallel velocity,

$$m \frac{dV_{||}}{dt} = - eE_{||}$$

and for the drift velocity,

$$V_{\perp} = \frac{\vec{E}x\vec{B}}{B^2}$$

The precession of **V** about **B** is computed in the drift frame where,

$$\frac{dV_{\perp}}{dt} = \vec{V}x\vec{W}$$

where $|W| = \frac{e|B|}{m}$ is the cyclotron frequency.

This drift approximation is used when the gyro motion is small compared to the zone size. When this is the case, resolving the gyro motion would not produce optimal accuracy to the trajectory because the local fields are not precisely known. The choice of when to use the drift approximation is made by comparing the local gyro radius to the zone size and switching to drift motion when the gyro radius is one-half of a mesh length.

3.3 Self-Consistent Sheaths

The sequence of calculations used to compute a self-consistent electron magnetosheath is listed below:

Step 1

Compute the potentials approximating the space charge density ignoring magnetic field effects.

$$\nabla^2\phi^0 = -\frac{\rho(E^0,\phi^0)}{\epsilon_0}$$

Step 2

Track electron trajectories from the sheath edge until one of the following happens: they hit the object; they exit the sheath; or they enter a trapped orbit. Use either the step push or drift methods depending on the field strengths. Use the fields from the latest potential solution.

$$\frac{d\vec{V}^i}{dt} = q\vec{E}^i + q\vec{V}x\vec{B}$$

$$\frac{d\vec{X}^i}{dt} = \vec{V}^i$$

Step 3

Using the time required for a particle to cross a cell, τ, increment the local plasma density for use in the next iteration of the potential solver.

$$\delta q^{i+1} = A_{sheath} J_{th} \tau$$

where A_{sheath} is the sheath area the superparticle represents.

Step 4

After tracking all superparticles from the sheath edge, recompute the potentials,

$$\nabla^2 \phi^{i+1} = - \frac{\rho(\{\phi^i\})}{\epsilon_o}$$

where $\rho(\{\phi^i\})$ represents the plasma density functional of the potentials at iteration i computed by particle tracking. We then loop back to the particle tracking phase, Step 2, and iterate until the collected current becomes stable. For most cases, stability can be defined in terms of the collected current.

4. POLAR 2.0 ELECTRON COLLECTION VALIDATION TESTS

To validate the current and potential algorithms in POLAR 2.0, we used as a standard test object a 10-cm sphere biased to 11,000 volts. The environment consisted of a 0.1-eV plasma with density $10^{11} m^{-3}$. This was used as a standard test object in the NASCAP/LEO code and in a 2 1/2-dimensional code. The 2 1/2-dimensional code used cylindrical symmetry to produce results that are valid for three dimensions, including magnetic field effects. We will present comparisons between POLAR 2.0 and these two codes.

The test object, shown in Fig. 4.1, is a QSPHERE (quasisphere) with a diameter of three mesh units. It has 26 faces composed of squares, rectangles, and triangles. This object is embedded in a nest of three grids which mesh sizes 0.536 m, 0.134 m, and 0.067 m as shown in Fig. 4.2. The outer grid, Grid 1, is 15 by 15 by 15 grid units. Grid 2 is 12 by 12 by 12 grid 2 units, or 3 by 3 by 3 grid 1 units. Grid 3, which contains the object, is 10 by 10 by 10 grid 3 units, or 5 by 5 by 5 grid 2 units. The QSPHERE is located at (4, 4, 4) in grid 3 units. Three grids were used

to test the grid nesting in POLAR 2.0. The grid ratios were chosen to be identical to the grid ratios used in the SPEAR I calculations.

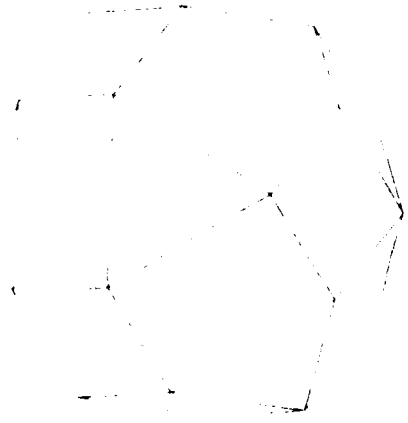

Fig. 4.1

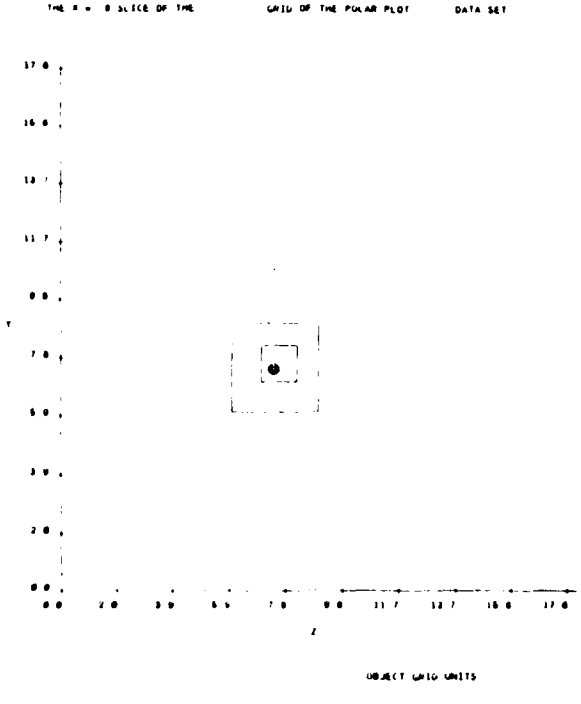

Fig. 4.2

4.1 Space Charge Sheaths without Magnetic Field Effects

For this test, potentials were computed using the analytical charge density, $\rho(E,\phi)$, during the first iteration and trajectory-determined charge density for subsequent iterations. First, we discuss a particle collection test which checked POLAR's ability to track electrons in combined magnetic and electric fields. This will be followed by a discussion of a self-consistent computation of the potentials.

Fig. 4.3 shows the potential contours computed by POLAR 2.0 using the analytic charge density; therefore, these potentials do not include magnetic field effects. Three contours are of particular interest. The first contour is the conventional sheath contour 0.67*kT. The second is the 0.75-volt contour computed by POLAR as the best estimate of the sheath edge. The third is the 22-volt contour that corresponds the potential, which will drop to zero due to spacecharge shielding in one 0.536-m zone.

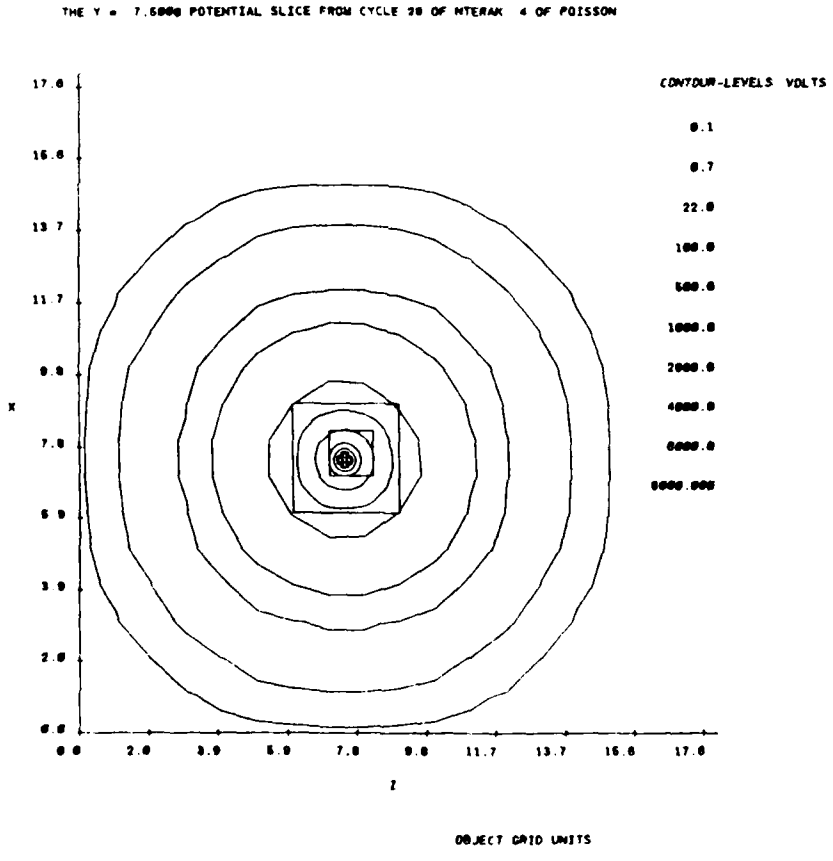

Fig. 4.3

$$\phi = \left[\frac{\delta x n^{\frac{1}{2}} T^{\frac{1}{4}}}{9.33}\right]^{\frac{4}{3}}$$

The analytical value for the sheath radius is 3.6 m. The radii of the three contours discussed above are 2.9 m, 3.4 m, 4.0 m, respectively. The 0.67*kT contour is much too large and would have been even larger had the grid been larger. The POLAR default 0.75-volt contour appears to be the best value for the sheath location. The 22-volt contour is more than one zone too small.

4.2 Magnetic Field Effects on Electron Collection

Fig. 4.4 shows trajectories for 20 electrons started 3.1 m from the 10-cm sphere. The purpose of this study was to check the particle tracking of electrons in a magnetic field.

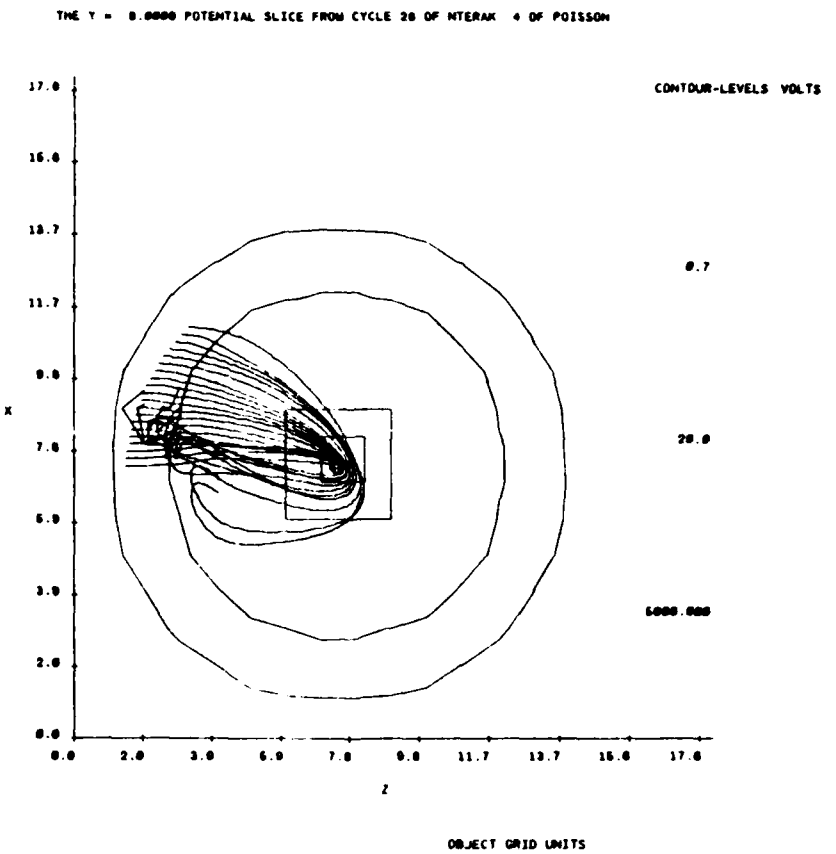

Fig. 4.4

As discussed, POLAR uses both a guiding center and a full particle tracking, depending on the electric and magnetic field strengths. The magnitude of the magnetic field was taken as 0.3 Gauss, which gives a thermal electron a gyroradius of 2.5 cm. This is much smaller than the mesh size of 53.6 cm in the outer grid. Even for the innermost grid, this is one-third of a zone. Table 4.1 below shows the input parameters for this SHONTL 2.0 run. The particles were started on an arc 3.1 m from the sphere, which are located at (7.2, 7.2, 7.2) grid units with 0.5 kT total energy and velocity directed in z. Compared with the sphere potential, the electrons are cold.

Table 4.1

Grid	X	Y	Z	Vx	Vy	Vz	Type	Energy	Comments
1	7.41	7.21	1.42	0	0	1	ELEC	0.5	Collected
1	7.61	7.21	1.44	0	0	1	ELEC	0.5	Collected
1	7.81	7.21	1.46	0	0	1	ELEC	0.5	Collected
1	8.01	7.21	1.49	0	0	1	ELEC	0.5	Collected
1	8.21	7.21	1.53	0	0	1	ELEC	0.5	Collected
1	8.41	7.21	1.58	0	0	1	ELEC	0.5	Collected
1	8.61	7.21	1.63	0	0	1	ELEC	0.5	Collected
1	8.81	7.21	1.69	0	0	1	ELEC	0.5	Collected
1	9.01	7.21	1.76	0	0	1	ELEC	0.5	Collected
1	9.21	7.21	1.84	0	0	1	ELEC	0.5	Collected
1	9.41	7.21	1.93	0	0	1	ELEC	0.5	Uncollected
1	9.61	7.21	2.03	0	0	1	ELEC	0.5	Uncollected
1	9.81	7.21	2.13	0	0	1	ELEC	0.5	Uncollected
1	10.01	7.21	2.25	0	0	1	ELEC	0.5	Uncollected
1	10.21	7.21	2.37	0	0	1	ELEC	0.5	Uncollected
1	10.41	7.21	2.51	0	0	1	ELEC	0.5	Uncollected
1	10.60	7.21	2.67	0	0	1	ELEC	0.5	Uncollected
1	10.80	7.21	2.83	0	0	1	ELEC	0.5	Uncollected
1	11.00	7.21	3.01	0	0	1	ELEC	0.5	Uncollected
1	11.20	7.21	3.22	0	0	1	ELEC	0.5	Uncollected

As can be seen in Fig. 4.4, the first 10 particles were collected by the object while the final 10 were not. This corresponds to a collection radius of R_B = 1.07 m. The limiting collection distance for a 10-cm sphere at 11,000 volts in a 0.3 Gauss magnetic field given by Parker and Murphy is 1.5 m.

4.3 Self-Consistent Electron Magnetosheath Calculation

The procedure to compute the self-consistent magnetosheath described in Section 2 was used for the 10-cm sphere biased to 11,000 volts. The calculation of the particle trajectories was taken up following the calculation of the space charge sheath shown in Fig. 4.3. During the first three iterations of the potential trajectory calculation, PWASON-CURREN, the number of left-right pushes in z was limited to three. This had the effect of limiting the lifetime of the particles in the sheath. Consequently, the shielding due to these particles was also reduced, creating a sheath slightly broader than it should have been. This in turn reduced the number of collectible orbits and, hence, the collected current. During the fourth and fifth iterations, the number of left-right pushes was increased to five and six, respectively. In Table 4.2, we list the convergence for this run.

To check the results, we developed a 2 1/2-dimensional computer code (2-dimensional coordinates and 3-dimensional velocities) and simulated this problem. The last column in Table 4.2 contains the results of this code. The code operates in cylindrical (r, z, θ) coordinates on a quadrilateral grid consisting of 90 spherical shells extending from the probe surface (0.1 m) to a radius of 7 m. Each shell had 25 angular divisions ranging from the z-axis to the r-axis. The $z = 0$ plane was treated as a mirror plane, and the $r = 7$m sphere was held fixed at zero potential.

Electrons were started along the magnetic field (z) direction from just inside the 7-m sphere with a radial spacing of 2.3 cm, and with current and velocity set to reproduce the one-sided plasma thermal current and one-half the ambient density. (Beyond the collection radius, the remaining half of the ambient density comes from electrons reflected from the $z = 0$ mirror plane.) Energy and canonical angular momentum were explicitly conserved at each particle time step. Each electron was followed until it either: 1. hit the probe; 2. escaped the grid; or 3. exceeded the limit of how many times it was allowed to bounce off the mirror plane. At each time step, the particle's charge was bilinearly shared to the nearby grid points.

Ion density was set to $ne^{-\frac{2\phi}{\pi\theta}}$.

Iterations consisted of alternately solving Poisson's equation and tracking particles in the resulting potentials to update the charge density. This process was continued

until steady state solutions were achieved. Potentials were constrained to be nonnegative; and in most runs, charge densities were constrained to be nonpositive. (The charge-density constraint affects potentials along field lines within the collection radius that in the quasineutral limit satisfy

$$ne^{-\frac{2\phi}{\pi\theta}} = 0.5\left[1 + \frac{\pi\phi}{\theta}\right]^{-\frac{1}{2}}$$

It had negligible effect on collected currents or on the potentials beyond the collection radius.

Table 4.2

Convergence history for 10-cm sphere

Iteration	Bounces	Current (mA)	2 1/2-D Code (mA)
1	3	-4.93	4.2
2	3	----	
3	3	-5.35	
4	5	-5.91	
5	6	-6.74	-6.7(10 bounces), -11(50 bounces)

As can be seen in the above table, the current in the POLAR 2.0 calculations is not fully converged. Iteration 1 uses potentials computed ignoring magnetic field effects but including space charge effects. It compares well with the 2 1/2-D results. The current is approaching the 6.7 mA result predicted by the 2 1/2-D self-consistent code for the 10-bounce case. The sheath current for Iteration 5 was 92 mA, so it is evident that the magnetic field is dramatically limiting the current collection. This is expected since the space charge sheath without a magnetic field is 3.6 m and the maximum collection radius given by canonical angular momentum conservation, the Parker-Murphy limit, is 1.5 m. Hence, this calculation is in the strong magnetic field limited regime.

Fig. 4.5 shows the potentials as they were at Iteration 5. As can be seen, the contours are compressed in the direction perpendicular to the magnetic field, which is in the z direction. This is due to particles with long lifetimes. The sheath dimension tries to adjust to fall within the magnetic limited collection radius.

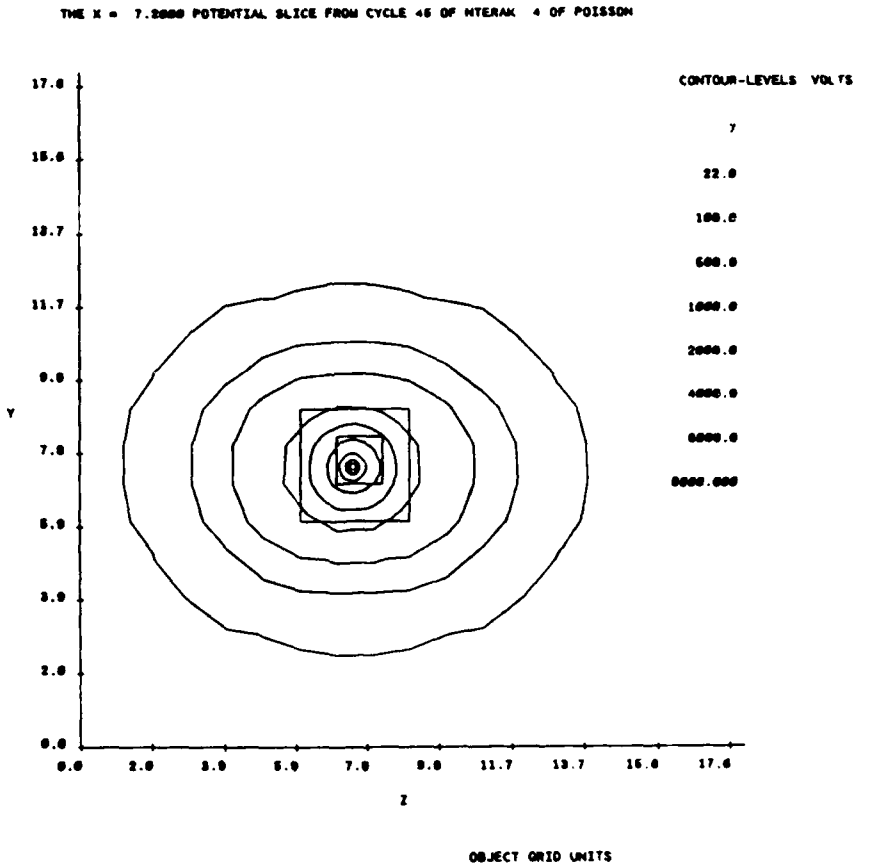

Fig. 4.5

5. POLAR 2.0 SPEAR I CALCULATIONS

This section contains a description of the SPEAR I object and grid structure used in the POLAR 2.0 calculations. Self-consistant magnetosheath calculations are presented for two SPEAR I voltage configurations.

5.1 SPEAR I Object and Grid Definition

The POLAR 2.0 SPEAR I calculations were performed in the object and computational grid structure shown in Fig. 5.1. The computational grid is composed of a total of 70.038 zones in four grids. The three inner grids provide increased resolution for

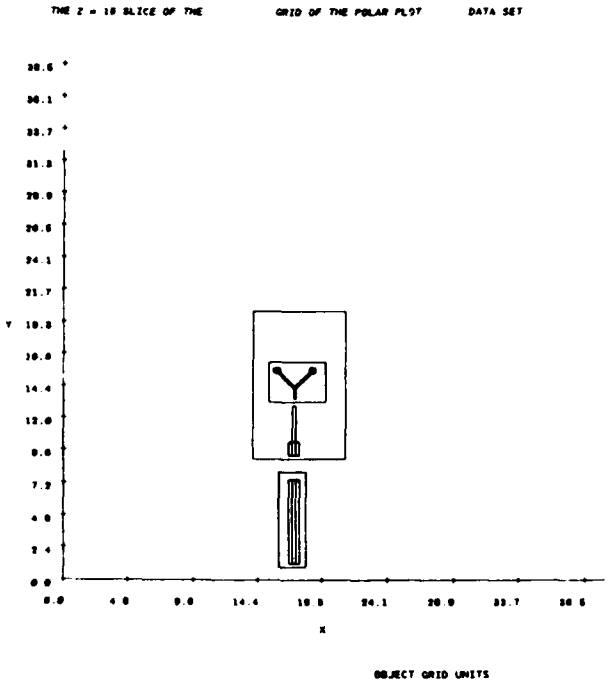
THE Z = 18 SLICE OF THE GRID OF THE POLAR PLOT DATA SET
X
OBJECT GRID UNITS

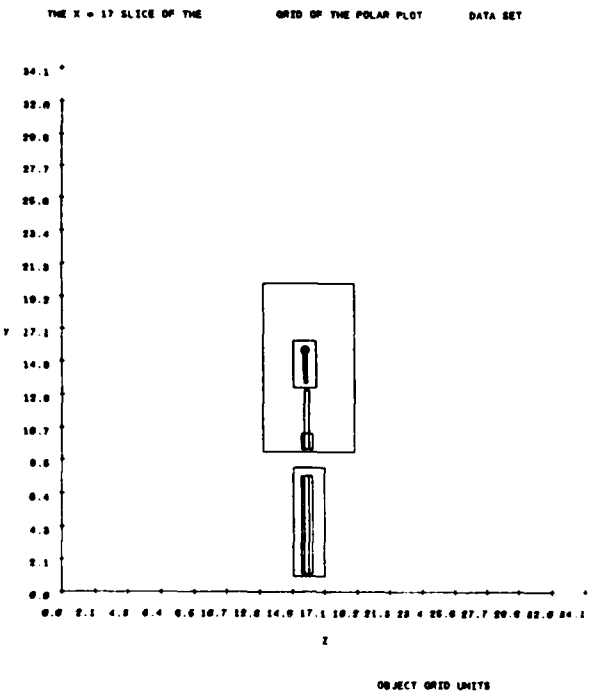
THE X = 17 SLICE OF THE GRID OF THE POLAR PLOT DATA SET
Z
OBJECT GRID UNITS

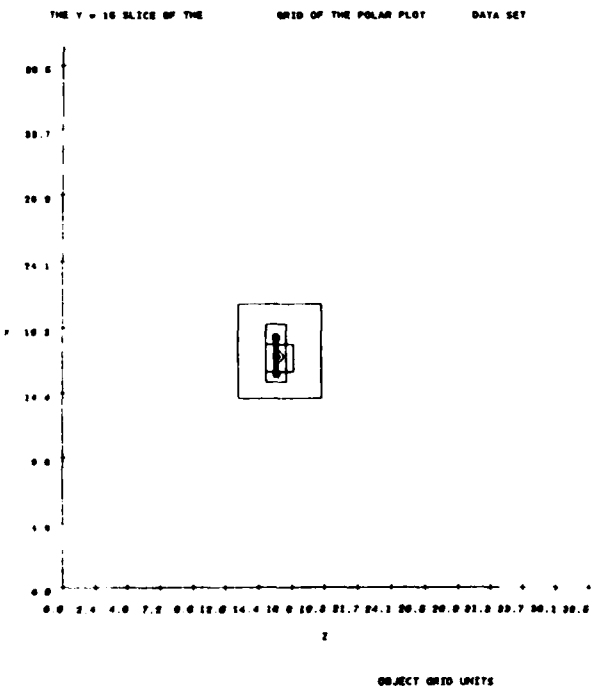
THE Y = 16 SLICE OF THE GRID OF THE POLAR PLOT DATA SET
Z
OBJECT GRID UNITS

Fig. 5.1

the rocket body (Grid 2), the plastic boom (Grid 3), and the bushings and spheres (Grid 4). Presently, POLAR 2.0 does not allow objects to cross grid boundaries and does not allow grids to share an edge. This restriction results in gaps in the SPEAR I object shown in the figure. These gaps are small and should not cause significant errors in the calculations. The gap between the bottom of the boom in Grid 4 and the top of the boom in Grid 3 is 20 cm, and the gap in the rocket body between Grids 2 and 3 is about 1 m.

Grid 1

Grid 1 is the outer grid and is designed to ensure that the entire space charge sheath will be contained within the computational space. It has dimensions 34 by 30 by 30 grid units and a mesh size of 0.5 m. This produces a computational space 13.6 m by 12 m by 12 m. This grid contains 30,110 (=30,600-1792/64-29568/64) computational zones.

Grid 2

Grid 2, the lower grid in Fig. 5.1, contains the rocket body. Details of the rocket body are shown in Fig. 5.2. The grid is 8 by 8 by 28 Grid 2 units, which is 2 by 2 by 6 Grid 1 units. Grid 2 has a grid ratio of four with respect to Grid 1, producing

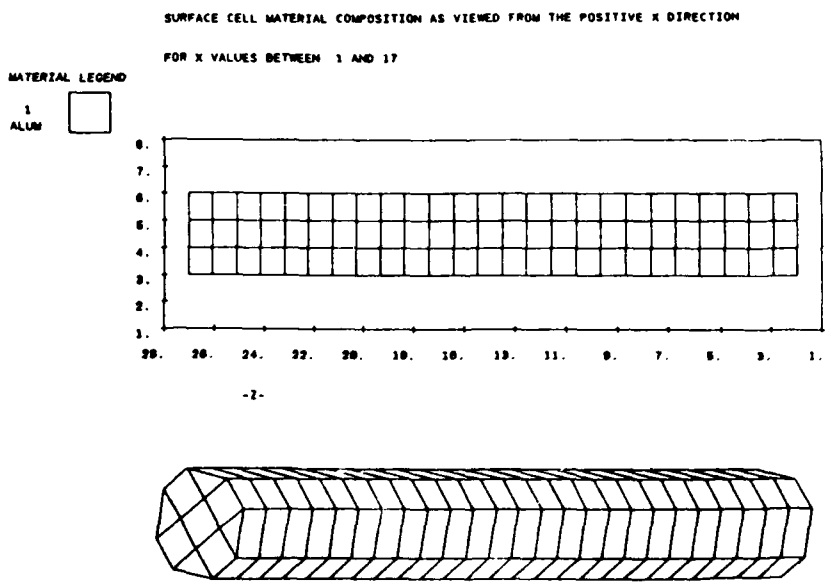

Fig. 5.2

a mesh size of 0.1 m and a computational size of 0.8 m by 0.8 m by 2.8 m, the lower portion of the rocket body in this grid. This grid contains 1,792 computational zones 2.6 m long.

Grid 3

Grid 3 is the upper grid shown in Fig. 5.1, which contains the upper rocket body and boom structure. This grid is detailed in Fig. 5.3 and the upper rocket body is detailed on Fig. 5.4. The grid is 28 by 44 by 24 Grid 3 units, which is 7 by 11 by 6 Grid 1 units. This grid has a grid ratio of four with respect to Grid 1, producing a mesh length of 0.1 m and a size of 2.8 m by 4.4 m by 2.4 m. This grid contains Grid 4, which has the detailed bushing and sphere structures. This grid contains 28,344 (=29568-9792/8) computational zones.

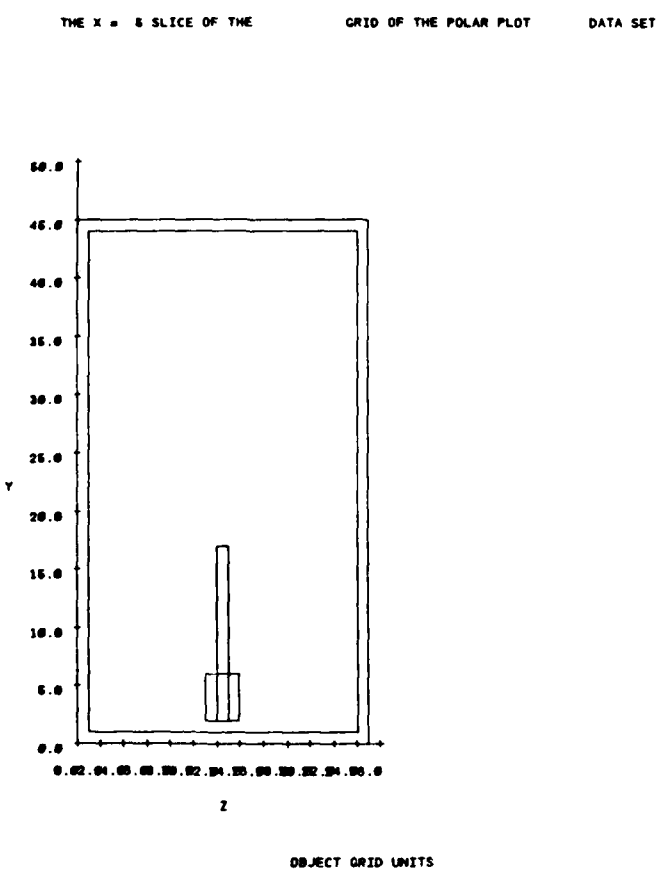

Fig. 5.3

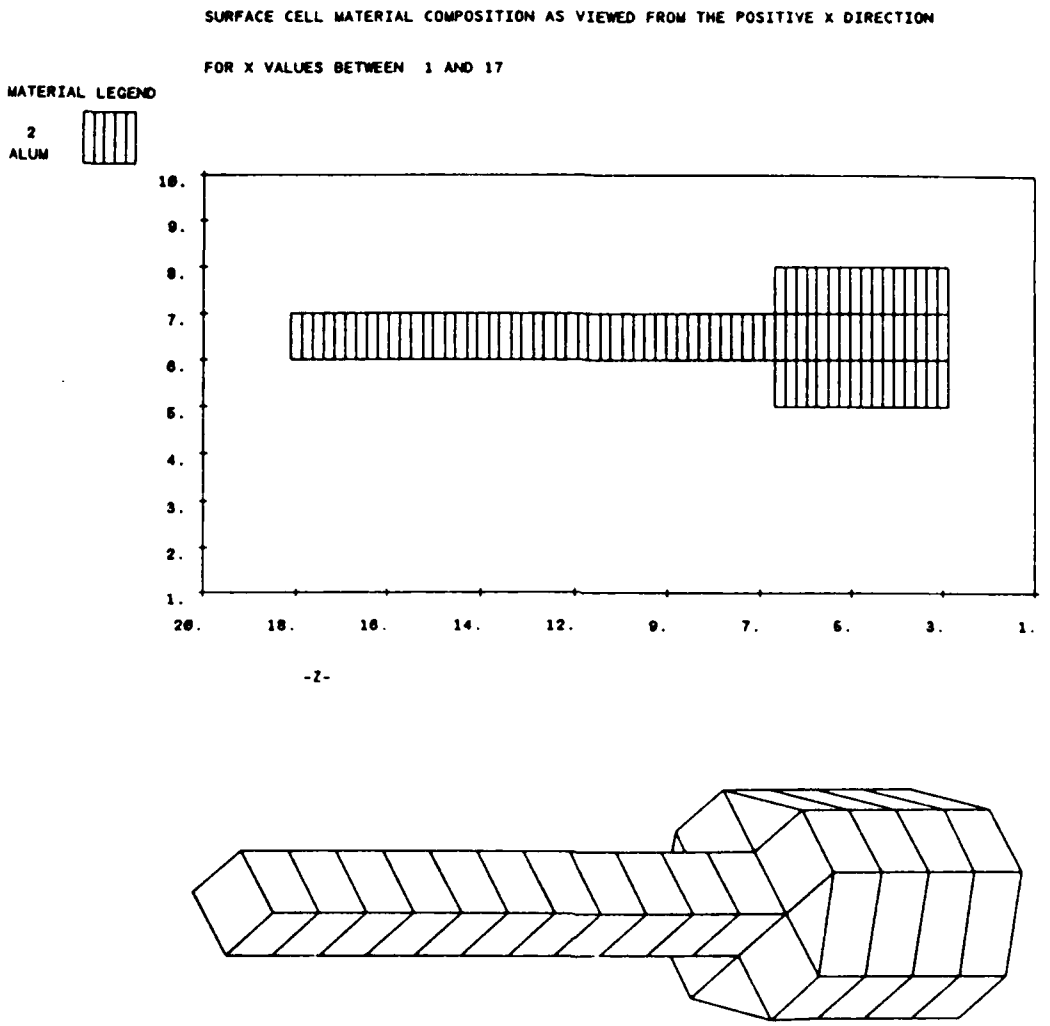

Fig. 5.4

Grid 4

The 10-cm spheres and resistive grating bushing are contained in Grid 4. A detailed view of this grid and the SPEAR I high voltage section is shown in Fig. 5.5. This grid is 34 by 24 by 12 Grid 4 units, which is 17 by 12 by 6 Grid 3 units. This grid contains 9,792 computational zones.

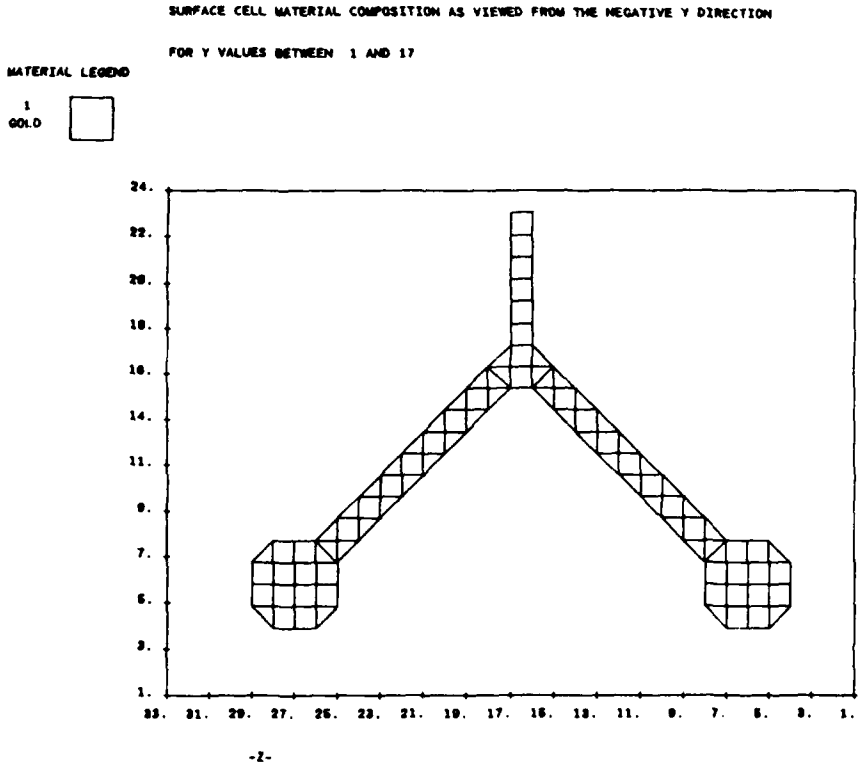

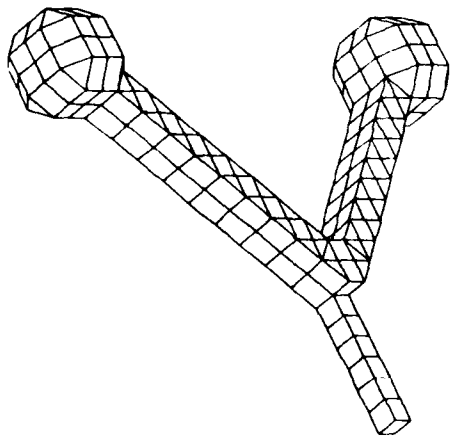

Fig. 5.5

Grid 4 has a grid ratio of two with respect to Grid 3 and a grid ratio of eight with respect to Grid 1. This results in a mesh size of 0.5 m for Grid 4. As can be seen in Fig. 5.5, a mesh size of 0.5 m produces 10-cm spheres separated by 1 m.

5.2 SPEAR I Calculations

POLAR 2.0 was used to calculate the currents to the SPEAR I rocket, bushings, and spheres for two voltage configurations. The first configuration was a 34,000 volt-12,000 volt combination. Down the bushings, the potentials were grated smoothly to zero at the joining point of the two supports. The plasma density was taken to be 1.e11 m^{-3} with a temperature of 0.1 eV. The second calculation was similar to the first case except that the voltages were scaled down to 8,900 volts for Sphere 1 and 3,100 volts for Sphere 2.

For both POLAR runs, the starting potential configuration was computed using the analytic form for the charge density, $\rho = \rho(\phi, E)$. As discussed, the form chosen gives the correct density for symmetric geometry in the absence of a magnetic field. Using this analytic approach for the zeroth stage of the calculations speeds the convergence of the later iterations by starting with a sheath that has approximately the correct length parallel to the magnetic field and slightly enlarged perpendicular to the magnetic field. Following this first calculation, a series of iterations were performed that consisted of particle tracking to determine the charge density (CURREN) and solving Poisson's equation to determine the potentials (PWASON). These iterations are continued until the self-consistent sheath, and hence, the currents to the SPEAR object are constant. Typically, this takes 5 to 10 iterations depending on the specifics of the calculation.

Case 1 34,000-12,000

To improve the stability of the calculation, the number of left-right pushes in Z, bounces, were increased as the calculation progressed. This had the effect of slowly reducing the width of the sheath in the perpendicular direction preventing unstable nonconvex sheath boundaries from forming. For each PWASON, nine space-charge iterations were performed to ensure convergence of the potentials. The number of bounces along with the total current to the object in each grid is shown below in Table 5.1.

Table 5.1

Convergence History for 34.000-12.000

Iteration	Bounces	Grid	Current
1	3	2	0.0000e+00 AMPS Sun 3/60
1	3	3	0.0000e+00 AMPS
1	3	4	-2.5854e-02 AMPS
2	3	2	0.0000e+00 AMPS Sun 3/60
2	3	3	0.0000e+00 AMPS
2	3	4	-2.2358e-02 AMPS
3	5	2	0.0000e+00 AMPS Sun 3/60
3	5	3	0.0000e+00 AMPS
3	5	4	-3.2196e-02 AMPS
5	5	2	0.0000e+00 AMPS Ridge 3200
5	5	3	0.0000e+00 AMPS
5	5	4	-3.6028e-02 AMPS
6	10	2	0.0000e+00 AMPS Ridge 3200
6	10	3	0.0000e+00 AMPS
6	10	4	-4.7793e-02 AMPS
7	10	2	0.0000e+00 AMPS Ridge 3200
7	10	3	0.0000e+00 AMPS
7	10	4	-4.6838e-02 AMPS
8	10	2	0.0000e+00 AMPS Ridge 3200
8	10	3	-1.6428e-05 AMPS
8	10	4	-4.8471e-02 AMPS

As can be seen from the table, the current has converged and remains constant for the last three iterations. The last column in the table indicates which computer performed the calculation. The calculation was initially run on a Sun 3/60, and then the data files transferred to the Ridge 3200 for completion of the calculations. The breakdown of currents to the object is given below in Table 5.2.

Table 5.2

Breakdown of Currents for 34.000-12.000 Volt Run

Object	Current (mA)
Sphere 1	-17.05
Sphere 2	-11.58
Bushing 1	-10.25
Bushing 2	-9.45
Rocket body	0.00
Plastic booms	-0.16
Sphere 1 and Bushing 1	-27.30
Sphere 2 and Bushing 2	-21.03

The total current is -48.49 mA.

The total current of 48.49 mA is more than 27 mA, which is what the Parker-Murphy limit would be for a single sphere with the same charge and an average potential of 23.000 volts. This is due to breaking of the symmetry and the current to the bushings. This collected current is much smaller than the sheath current for this same effective sphere, which is 480 mA. Fig. 5.6 shows the converged potentials for this voltage configuration.

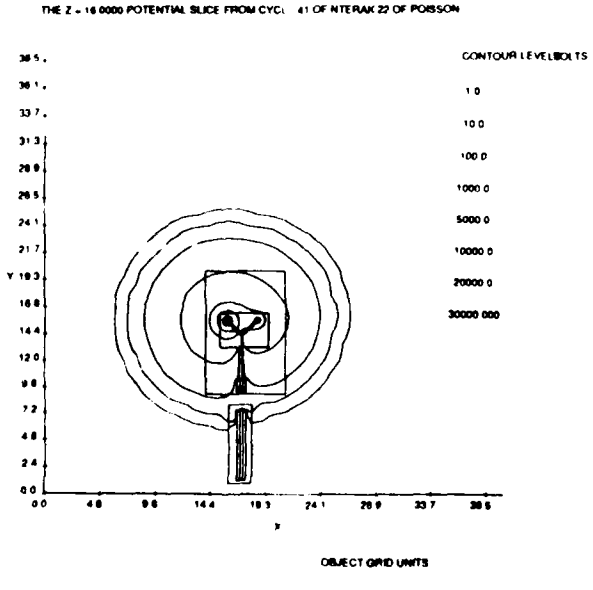

Fig. 5.6 Converged potentials for 34.000-12.000 volt run.

Case 2 8,900-3,100

Following the zeroth calculation using the analytic form for the charge density, six CURREN-PWASON iterations were performed. The sequence of CURREN runs used the following number of bounces: 3, 3, 5, 10, 10. For each PWASON, nine space-charge iterations were performed to ensure that the potentials were converged. In addition, the potentials were examined after each iteration to determine the quality of the potential solution. The convergence of the total current collected for each grid is shown in Table 5.3 and the breakdown of the currents to the SPEAR I object are shown in Table 5.4 below:

Table 5.3

Convergence History for 8,900-3,100

Iteration	Bounces	Grid	Current
1	3	1	0.0000e+00 AMPS
1	3	2	0.0000e+00 AMPS
1	3	3	-1.1168e-02 AMPS
2	3	1	0.0000e+00 AMPS
2	3	2	0.0000e+00 AMPS
2	3	3	-1.4087e-02 AMPS
3	5	1	0.0000e+00 AMPS
3	5	2	0.0000e+00 AMPS
3	5	3	-2.1766e-02 AMPS
4	10	1	0.0000e+00 AMPS
4	10	2	-2.1683e-06 AMPS
4	10	3	-3.0847e-02 AMPS
5	10	1	0.0000e+00 AMPS
5	10	2	0.0000e+00 AMPS
5	10	3	-2.7342e-02 AMPS
6	10	1	0.0000e+00 AMPS
6	10	2	0.0000e+00 AMPS
6	10	3	-3.2653e-02 AMPS

Table 5.4

Breakdown of Currents for 8,900-3,100 Volt Run

Object	Current (mA)
Sphere 1	-12.12
Sphere 2	-10.32
Bushing 1	-5.88
Bushing 2	-4.25
Rocket body	0.00
Plastic booms	-0.09
Sphere 1 and Bushing 1	-18.00
Sphere 2 and Bushing 2	-14.57

The total current is -32.65.

The total current of 32.65 mA is more than 14 mA, which is what the Parker-Murphy limit would be for a single sphere with the same charge and an average potential of 23,000 volts. This is due to breaking of the symmetry and the current to the bushings. This collected current is much smaller than the sheath current for this same effective sphere, which is 156 mA. Fig. 5.7 shows the converged potentials for this voltage configuration.

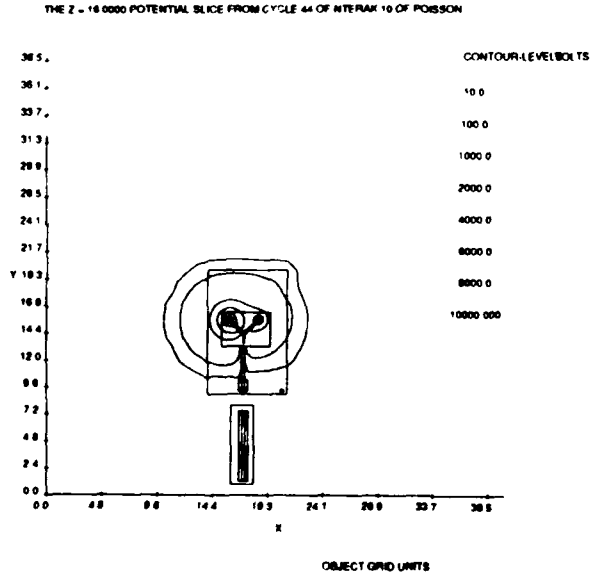

Fig. 5.7 Converged potentials for 8,900-3,100 volt run.

6. COMPARISONS POLAR AND NASCAP/LEO SPEAR I CURRENT COLLECTION CALCULATIONS

Calculations performed using both the POLAR 2.0 and NASCAP/LEO codes showed basic agreement with magnetic limited spherical probe theory for the total current. All calculations were performed for ne = $10^{11}m^{-3}$, Te = 0.1eV, and b = 0.4 Gauss.

Table 6.1 shows how the self-consistent space charge effects in the POLAR 2.0 calculations increase the currents by about a factor of two over the NASCAP/LEO results. Both POLAR 2.0 and NASCAP/LEO predict currents dramatically reduced by the magnetic field: for example, in the absence of magnetic fields, 0.47 amperes would be collected by SPEAR I for the 46,000 volt, f = 1/3 case. The initial iteration in the POLAR 2.0 calculation gave total currents that were almost identical with those from NASCAP/LEO.

Table 6.1

Total currents in amperes collected by both spheres for a voltage ratio of one-third. POLAR 2.0 includes both 3-dimensional geometry and self-consistent space charge.

Voltage	PM	POLAR	NASCAP/LEO
12,000	1.25e-2	3.26e-2	1.41e-2
46,000	2.64e-2	4.85e-2	2.80e-2

Table 6.2 shows how the current is distributed between the two spheres when one sphere has about three times the potential of the other sphere. For the lowest potential, the currents are divided much like independent probe calculations would predict. In the NASCAP/LEO calculations, as the potentials increase, the fraction going to the higher potential sphere increases. We attribute this to an overlap of the sheaths: electrons in the shared region are preferentially collected by the higher potential sphere. However, in the POLAR 2.0 calculations, the fraction to the lower potential sphere initially remains near the independent sphere results. As the magnetic field compresses the sheath, the collection by the two spheres becomes more even. This difference between POLAR 2.0 and NASCAP/LEO has not been tracked down.

Both particle pushing routines have been tested; the difference is more likely due to differences in the computational object definition or small differences in the potential profiles. More work is needed to be able to extrapolate SPEAR I results to SPEAR II.

Table 6.2

Current ratios between the two spheres when the voltage ratio between the spheres is one-third. Values listed are the ratios of the smaller current to the larger current.

Voltage	PM	POLAR	NASCAP/LEO
12.000	0.59	0.81	0.533
46.000	0.60	0.77	0.592

7. SUMMARY

Further calculations are planned to test the POLAR 2.0 code. The charge module, electric field boundary conditions, and wake module have not been tested. Furthermore, differences were found between the NASCAP/LEO and the POLAR 2.0 codes in the distribution of currents to the SPEAR I rocket. Because of the large sheath sizes in the calculations, these differences could have resulted from small differences in the potentials and object definitions. This needs further study.

The POLAR 2.0 support code, SHONTL, is not completed. Presently, potential plots and tabular data can be displayed; but the full range of plots has not been fully implemented. In addition, an Iris version of the code that will provide convenient viewing capability is being prepared.